International Journal of Thermal Sciences 49 (2010) 1073–1085

Contents lists available at ScienceDirect

International Journal of Thermal Sciences

journal homepage: www.elsevier.com/locate/ijts

Scale effects on flow boiling heat transfer in microchannels: A fundamental perspective

Satish G. Kandlikar

Mechanical Engineering Department, Rochester Institute of Technology, Rochester, NY 14623, USA

ARTICLE INFO

Article history:
Received 23 October 2009
Received in revised form
20 December 2009
Accepted 25 December 2009
Available online 20 February 2010

Keywords:
Flow boiling
Boiling
Microchannels
Mechanisms
Scale
Scaling

ABSTRACT

Flow boiling in microchannels has received considerable attention from researchers worldwide in the last decade. A scaling analysis is presented to identify the relative effects of different forces on the boiling process at microscale. Based on this scaling analysis, the flow pattern transitions and stability for flow boiling of water and FC-77 are evaluated. From the insight gained through the careful visualization and thermal measurements by previous investigators, similarities between heat transfer around a nucleating bubble in pool boiling and in the elongated bubble/slug flow pattern in flow boiling are brought out. The roles of microlayer evaporation and transient conduction/microconvection are discussed. Furthermore, it is pointed out that the convective contribution cannot be ruled out on the basis of experimental data which shows no dependence of heat transfer coefficient on mass flow rate, since the low liquid flow rate during flow boiling in microchannels at low qualities leads to laminar flow, where heat transfer coefficient is essentially independent of the mass flow rate. Specific suggestions for future research to enhance the boiling heat transfer in microchannels are also provided.

1. Introduction

Flow boiling is a highly efficient mode of heat removal. At macroscale, it provides superior performance compared to single-phase or pool boiling heat transfer. At microscale, however, this paradigm is now open to question due to recent advances in single-phase heat transfer with water in enhanced microchannels that have yielded heat transfer coefficients in excess of 500,000 W/m^2 °C and are able to remove heat fluxes of 500 W/cm^2 [1,2]. Such high values have not yet been reported under flow boiling conditions in microchannels. The added complexity of a flow boiling loop with microchannels may not be justified unless the performance is better than that of a simple pool boiling system or a single-phase system. This article aims at understanding the effects of microscale on flow boiling heat transfer in an attempt to identify methods to improve the heat transfer performance to accommodate heat fluxes (beyond 1 kW/cm^2) higher than that are possible today with liquid cooling. Excellent reviews have been published periodically on this evolving topic [3–11].

Understanding the transport phenomena occurring at the wall–fluid interface is of great interest in developing enhanced heat transfer surfaces. In pool boiling for example, several techniques to provide re-entrant nucleation cavities of appropriate mouth opening and surface substructure to trap gases have yielded significant enhancement in heat transfer [12]. In macroscale flow boiling, high performance compact evaporator surfaces have been developed through extensive experimentation, e.g. compact plate-fin evaporators [13] and microfin tubes [14].

A number of recent research efforts on flow boiling in microchannels are focused on understanding the underlying mechanisms [4,5,15–24]. To further explore the scale effects on flow boiling at microscale, a scaling analysis is first presented in this paper to identify the effects of various forces. Drawing on some of the earlier published work, heat transfer in the vicinity of advancing and receding menisci is then analyzed. Based on this analysis and some of the recent work by other investigators on the high-speed visualization and localized thermal measurements made at the base of a nucleating bubble in pool boiling, a comparison is made between the heat transfer mechanisms during pool boiling and flow boiling in microchannels. In flow boiling, a number of useful criteria are proposed in the literature to characterize the microscale effects such as bubble confinement [25,26]. Microchannels in this paper are defined as channels with hydraulic diameters smaller than about 200 μm following the classification by Kandlikar and Grande [27].

1.1. Useful parametric ranges for flow boiling in microchannels

Flow boiling studies have been conducted in recent years in an effort to meet the high heat flux removal requirements of IC chips. Employing flow boiling in ultra-compact evaporators for high heat

E-mail address: sgkeme@rit.edu

1290-0729/$ – see front matter © 2010 Elsevier Masson SAS. All rights reserved.
doi:10.1016/j.ijthermalsci.2009.12.016

Nomenclature

A_c	channel cross-sectional area, m^2
Bo	Boiling number, defined by Eq. (11)
Ca	Capillary number, defined by Eq. (15)
D	diameter, m
F'	Force per unit length, N/m
F''	Force per unit area, N/m^2
g	acceleration due to gravity, m/s^2
G	mass flux, kg/m^2s
h_{fg}	latent heat of vaporization, J/kg
K_1	non-dimensional number by Kandlikar [17], defined by Eq. (13)
L	channel length, m
P	Perimeter, m
q	heat flux, W/m^2
V	mean fluid velocity, m/s
Δx	change in quality
We	Weber number, defined by Eq. (14)

Greek symbols

δ	liquid film thickness, m
θ	contact angle
μ	viscosity, kg/ms
ρ	density of the fluid, kg/m^3
τ	shear stress, N/m^2

Subscripts

g	gravity
h	hydraulic
L	liquid
M	evaporation momentum
i	inertia
v	vapor
σ	surface tension
τ	shear

transfer performance is also attractive in many other applications, such as automotive evaporators and air liquefaction systems. It is thus important to identify the relevant ranges of parameters employed in these applications.

In chip cooling applications, heat fluxes up to about 50–80 W/cm^2 can be handled with aggressive air cooling techniques employing ducted air flow through compact heat exchanger passages. Liquid cooling has been effectively applied to remove heat fluxes up to around 500 W/cm^2 [1]. Using refrigerated liquid, heat flux levels can be further enhanced. There are efforts under way in many academic and industrial research centers to dissipate heat fluxes beyond 1 kW/cm^2 with single-phase cooling. However, the practical constraints in providing complex headers and employing large pressure drops will eventually limit the single-phase liquid cooling option. A much higher performance would be expected from a flow boiling system to become preferable over a single-phase cooling system. Currently, some of the issues related to instabilities have been resolved in flow boiling systems, but higher heat fluxes (on the order of 1 kW/cm^2 and beyond) seem to be difficult to achieve. This paper addresses some of the underlying issues in an attempt to extend the heat removal limits of flow boiling systems employing microchannels.

2. Scale effect on heat transfer and two-phase flow

2.1. Scale effect on inertia, surface tension, shear, gravity, and evaporation momentum forces

Flow boiling heat transfer is intimately linked to the wall transport in the presence of a liquid–vapor interface. There are five major forces that come into play. As the channel diameter decreases, the actual magnitudes of all of these forces will go down. Since the relative magnitudes of these forces are of interest rather than their actual values, the forces are normalized with respect to the channel size. The normalization may be done using the volume, cross-sectional area or perimeter (diameter) of the microchannel. Since local values are of interest, normalization with respect to volume will not provide such information. The forces are expressed in two forms: (i) force per unit length is useful in considering a force balance on a bubble on the wall or for analyzing CHF condition at the contact line, and (ii) force per unit area is useful for studying the effect on flow patterns, heat transfer and flow instability. The resulting expressions are presented below:

2.1.1. Inertia force

The inertia force F_i acts over the channel cross-section. Normalizing this force per unit length (F_i') and per unit area (F_i'') we get:

$$F_i' \sim \rho V^2 \frac{D^2}{D} = \frac{G^2 D}{\rho} \tag{1}$$

$$F_i'' \sim \rho V^2 \frac{D^2}{D^2} = \frac{G^2}{\rho} \tag{2}$$

where ρ is the density of the fluid (liquid density is appropriate prior to nucleation, and average density is appropriate in two-phase flow), V is the mean fluid velocity, and G is the mass flux.

2.1.2. Surface tension force

Surface tension force is considered with the liquid–vapor interface across the entire cross-section. The surface tension force per unit length (F_σ') and per unit area (F_σ'') are given by:

$$F_\sigma' \sim \frac{\sigma \cos(\theta) D}{D} \sim \sigma \tag{3}$$

$$F_\sigma'' \sim \frac{\sigma \cos(\theta) D}{D^2} \sim \frac{\sigma}{D} \tag{4}$$

where σ is the surface tension and θ is the contact angle of the liquid–vapor interface on the channel wall.

2.1.3. Shear force

Shear force on a representative surface of length equal to the channel diameter is employed. The shear force per unit length (F_τ') and per unit area (F_τ'') are given by:

$$F_\tau' \sim \frac{\frac{\mu V}{D} D^2}{D} = \mu V = \frac{\mu G}{\rho} \tag{5}$$

$$F_\tau'' \sim \frac{\frac{\mu V}{D} D^2}{D^2} = \frac{\mu V}{D} = \frac{\mu G}{\rho D} \tag{6}$$

where μ is the fluid viscosity. Under the two-phase conditions, the choice of fluid properties depends on the fluid that is in contact

with the channel wall. Prior to nucleation, liquid properties are appropriate.

2.1.4. Gravity (buoyancy) force

The buoyancy force results from the difference in the vapor–liquid densities, and is a body force, similar to the inertia force. It is expressed per unit length (F_g') and per unit area (F_g'') by the following equations:

$$F_g' \sim \frac{(\rho_L - \rho_v)gD^3}{D} = (\rho_L - \rho_v)gD^2 \tag{7}$$

$$F_g'' \sim \frac{(\rho_L - \rho_v)gD^3}{D^2} = (\rho_L - \rho_v)gD \tag{8}$$

where g is the acceleration due to gravity.

2.1.5. Evaporation momentum force

As the liquid evaporates, there is a force exerted at the evaporating interface due to the change in momentum caused by the increase in velocity as the liquid phase changes into vapor phase. The following expression gives the magnitude of this force per unit length (F_M') and per unit area (F_M''):

$$F_M' \sim \left(\frac{q}{h_{fg}}\right)^2 \frac{D}{\rho_V} \tag{9}$$

$$F_M'' \sim \left(\frac{q}{h_{fg}}\right)^2 \frac{1}{\rho_V} \tag{10}$$

where q is the wall heat flux and h_{fg} is the latent heat of vaporization. The evaporation momentum force acts on the evaporating interface and plays a major role in its motion. This force depends on the applied heat flux and has been employed in modeling the CHF phenomenon in pool boiling [28].

The relative magnitudes of these forces are plotted using the forces per unit area to illustrate the effect of changing scale (diameter). Fig. 1 shows the relative magnitudes of these forces for water at atmospheric pressure and channel diameters ranging from 10 mm down to 10 μm at a relatively low flow rate of $G = 50$ kg/m^{2}s and $q = 1$ MW/m^2. The inertia and shear forces are calculated using all liquid flow. At 10 mm, the gravitational forces are dominant. The shear force appears to be several orders of magnitudes lower than the inertia force, but in reality, shear force scales differently as it is applied over the tube wall, whereas other forces are either body forces or are applied over the liquid–vapor interface. It may be recalled that the ratio of inertia to shear force results in Reynolds number, which is a large number in macroscale heat transfer applications. The Reynolds number therefore represents an appropriate scaling factor for the shear and inertia forces. For the low flow rate depicted in Fig. 1, surface tension represents an important force during flow boiling in microchannels. As the diameter becomes smaller, the surface tension and viscous forces increase and become dominant.

The effect of mass flux on the forces can be seen in Figs. 2 and 3, which are drawn for $G = 200$ and 1000 kg/m^{2}s, respectively. Such high mass fluxes have been investigated in literature; for example the highest mass flux employed by Steinke and Kandlikar [29] with water was 1782 kg/m^{2}s, and recently Kosar et al. [30] employed extremely high mass fluxes up to 53,000 kg/m^{2}s in circular microchannels ranging from 127 to 254 μm in diameter in their CHF studies. It is seen that as the mass flux increases, the relative importance of inertia goes up significantly, while shear forces also become larger. Gravity, which is a body force, remains insignificant compared to shear and inertia forces for channels below about 100–200 μm diameter.

The evaporation momentum force depends on the applied heat flux. To show the changes in this force at high evaporation rates, Fig. 1 with $q = 1$ MW/m^2 is replotted in Fig. 4 with $q = 10$ MW/m^2. Comparing Figs. 1 and 4, it is seen that the evaporation momentum force becomes quite large, exceeding the inertia and shear forces. The large evaporation momentum force at high evaporation rates encountered at the inception of nucleation is responsible for the rapid interface movement, sometimes causing reversed flow in microchannels.

Fig. 5 shows a similar force representation for R-123 at $G = 200$ kg/m^{2}s and $q = 1$ MW/m^2. It is seen that the surface tension forces are reduced due to the lower surface tension of R-123 and the evaporation momentum force is also reduced due to the lower latent heat. Nevertheless, surface tension comes out as the dominant force, with inertia forces being the second most significant force. However, a note on the role of surface tension force is warranted.

The surface tension force acting at the contact line of the three phases (during rewetting on a dry surface) is applied through the contact angle. The wettability of the channel walls and the dynamic and time-dependent behavior of the contact angle are relevant physical considerations. Secondly, the nature of liquid–vapor

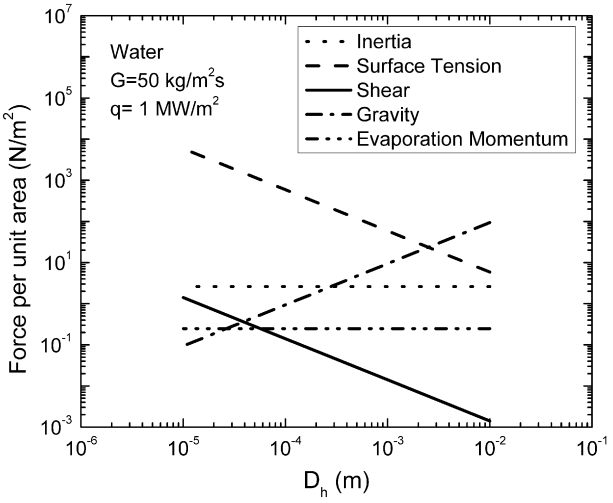

Fig. 1. Scale effect of tube diameter on various forces during flow boiling of water, $G = 50$ kg/m^{2}s, $q = 1$ MW/m^2.

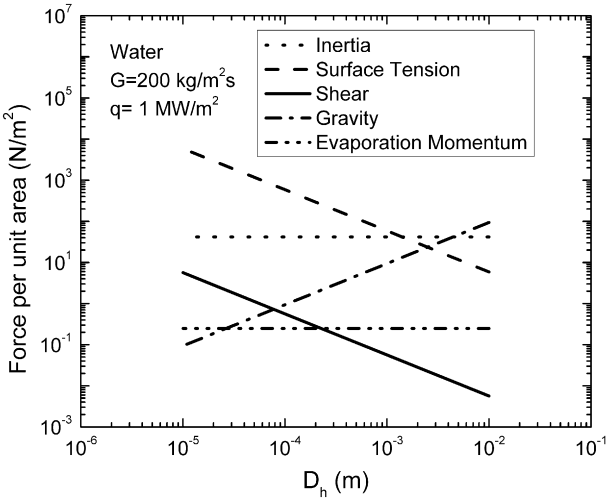

Fig. 2. Scale effect of tube diameter on various forces during flow boiling of water, $G = 200$ kg/m^{2}s, $q = 1$ MW/m^2.

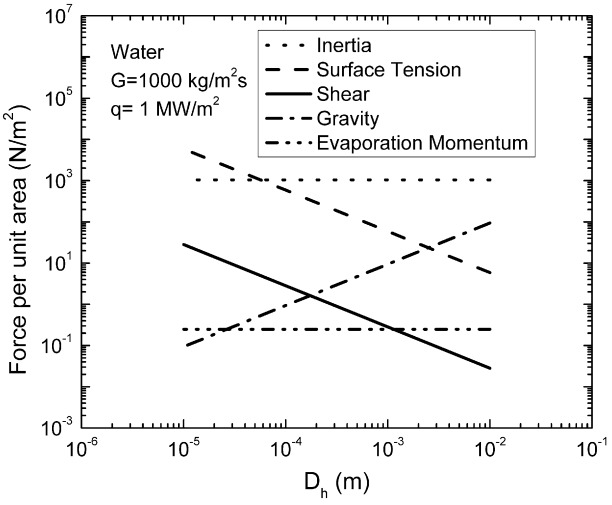

Fig. 3. Scale effect of tube diameter on various forces during flow boiling of water, $G = 1000$ kg/m^{2}s, $q = 1$ MW/m^2.

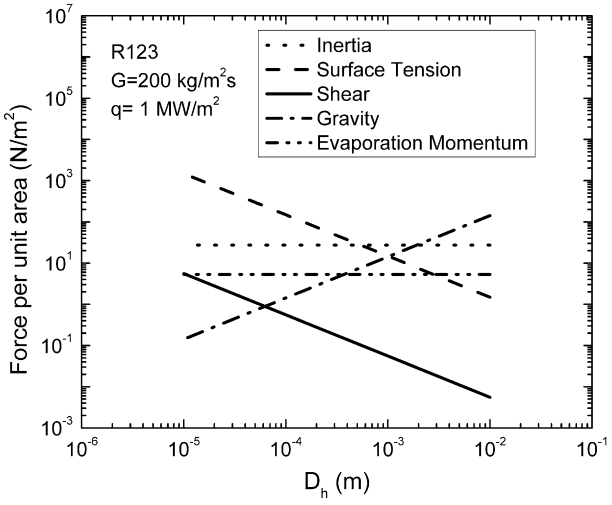

Fig. 5. Scale effect of tube diameter on various forces during flow boiling of R-123, $G = 200$ kg/m^{2}s, $q = 1$ MW/m^2.

interface during the two-phase flow is of critical importance. For illustration, consider a small bubble 10 μm in diameter. When this bubble is attached to the wall, the strong surface tension forces would require significant shear and inertia forces to dislodge it from the wall and eject it in the flow. However, when this bubble is detached and is flowing, its influence on the flow is quite different and relatively small. Small diameter bubbles generally do not coalesce easily and tend to grow as large confined bubbles in the channels for water as seen by Tange et al. [31]. For refrigerants, the coalescence may be easier due to lower surface tension forces. The growth of the bubbles in the flow provides a relaxation mechanism for the liquid superheat in the bulk flow. Advancing this concept, microbubble emission in pool boiling was accomplished by Li et al. [32] by incorporating micron-sized cavities and developing nanostructures of pin fins oriented obliquely to the heating surface.

2.2. Scaling parameters – relevant non-dimensional groups in microscale flow boiling

As pointed out earlier, although the magnitudes of inertia and shear forces are quite different, they scale differently in the near-wall region, which is of primary interest in flow boiling. The ratio of the inertia and shear forces results in the Reynolds number, which is used extensively in fluid flow and convective heat transfer studies. Reynolds number is much greater than unity in engineering heat transfer and fluid flow applications, and provides the correct scaling factor for these two forces.

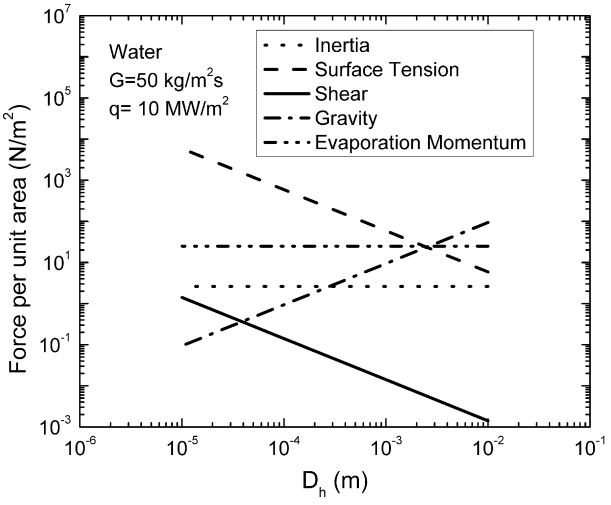

Fig. 4. Scale effect of tube diameter on various forces during flow boiling of water, $G = 50$ kg/m^{2}s, $q = 10$ MW/m^2.

In flow boiling heat transfer, use of empirically derived non-dimensional groups is quite common. The earliest group used in two-phase flow pressure drop modeling is the Martinelli parameter, X_{tt}, which represents the ratio of the two-phase flow pressure drop to the pressure drop with only single-phase gas or liquid flowing in the entire tube. This parameter has found widespread empirical acceptance in flow boiling pressure drop as well as heat transfer modeling. A detailed discussion of empirical and other non-dimensional numbers is provided in ref. [17].

Another empirical parameter that is used extensively is the boiling number, Bo, defined as:

$$\mathrm{Bo} = \frac{q}{Gh_{\mathrm{fg}}} \tag{11}$$

Boiling number represents the ratio of heat added to that which is required to evaporate liquid flow into vapor. However, it does not account for the tube the entire diameter effect and thus has a different influence depending on the channel dimensions. From an evaporator design standpoint, comparing the heat input to the maximum energy that can be carried away by evaporation for a prescribed change in quality, the maximum boiling number that can be realized is given by the following relation for a circular channel:

$$\mathrm{Bo}_{\max} = \frac{A_c \Delta x}{PL} = \frac{0.25\Delta x}{(L/D_h)} \tag{12}$$

where L is the channel length, A_c is the channel cross-sectional area, and Δx is the change in quality from inlet to the exit of the channel. For an exit quality of 1, exceeding the $\mathrm{Bo}_{\max}$ value will lead to an equilibrium quality of greater than 1 within the channel. CHF condition will further limit this value.

While studying nucleation and bubble removal processes, a comparison of the inertia and evaporation momentum forces is useful and results in the following non-dimensional number by Kandlikar, K_1, [17] which is derived from theoretical force balance considerations:

$$K_1 = \left(\frac{q''}{Gh_{fg}}\right)^2 \frac{\rho_L}{\rho_V} = Bo^2 \frac{\rho_L}{\rho_V} \quad (13)$$

While the boiling number represents a non-dimensional quantity incorporating the heat and mass fluxes, K_1 represents the ratio of evaporation momentum to inertia forces encountered during boiling at microscale. The rate of volumetric change during evaporation under a given set of heat and mass fluxes is also taken into account in K_1. From Eqs. (12) and (13), it is seen that Bo appears with the non-dimensional L/D_h ratio in the overall energy transfer analysis, and with the density ratio ρ_L/ρ_V during transport processes at the interface.

Since the gravitational forces have negligible influence during internal flow boiling at microscale, the other two groups that combine surface tension force with inertia (Weber number, We) and viscous (Capillary number, Ca) forces play an important role.

$$We = \frac{LG^2}{\rho\sigma} \quad (14)$$

$$Ca = \frac{\mu V}{\sigma} \quad (15)$$

However, the effects of the shear stress on the flow characteristics is still expected to be low as the shear stress is quite small compared to the other forces. It may be noted that the effect of surface tension is manifested at the contact line as well as in defining the shape of the liquid–vapor interface.

2.3. Flow patterns during flow boiling in microchannels

The interplay among the forces at the liquid–vapor interfaces due to surface tension, inertia, shear, gravity, bubble nucleation and evaporation is responsible for the flow patterns observed during flow boiling. As seen from Figs. 1–4, for larger tube diameters, above 3 mm, the gravitational forces are dominant. For these macroscale tubes, a stratified flow pattern is observed at lower total mass fluxes during two-phase flow in evaporators. The annular flow pattern also becomes asymmetric in horizontal channels. As the diameter becomes smaller, the gravitational effects become smaller and the inertia forces favor the annular flow. Similarly, the churn flow pattern seen in larger diameter tubes becomes less prevalent as the channel diameter decreases, and quickly transforms into slug or annular flow patterns.

The role of heat flux becomes more important in the hydrodynamics of two-phase flow at microscale. The bubble nucleation process is initiated by the large degree of wall superheat and negative subcooling (bulk liquid becomes superheated) [22]. The liquid–vapor interface of a growing bubble provides a relaxation mechanism in the superheated bulk liquid through evaporation. This relaxation mechanism represents an important heat transfer enhancement mode by reducing the effective temperature of the bulk liquid for single-phase convection (or transient conduction in the slug as will be shown later) from the heated channel walls.

The effect of channel dimensions on the more prevalent flow patterns in microchannels are presented next on the basis of experimental observations reported in the literature.

2.3.1. Bubbly flow

Bubbles generated at the wall detach and move in the bulk flow. For macrochannels, the bulk liquid reaches the saturation temperature and the bubbles flow randomly in the cross-section. As the channel diameter decreases, the bubbles are seen to flow more regularly in the center and assume elongated shape as found by Zhao and Bi [33] during the adiabatic flow of air and water for triangular channels of hydraulic diameters of 2.886, 1.443 and 0.866 mm. Sobierska et al. [34] observed bubbly flow in the subcooled region and at very low qualities for rectangular channels of $D_h = 0.48$ and 1.86 mm. Revellin et al. [35] observed single streams of bubbles which grew in size for R-134a and R-245fa in channels of $D_h = 0.5$ mm and are seen only at low mass fluxes. For microchannels with $D_h = 100$ μm, Kawahara et al. [36] noted that bubbly flow was not seen for air–water mixture as well. Wang et al. [37] observed bubbly to slug flow transition at high heat fluxes with very short slug lengths. Harirchian and Garimella [38] observed that the bubbly flow is observed for channels 400 μm and wider, but is suppressed in 100 μm diameter microchannels.

2.3.2. Explosive bubble growth

A number of investigators working on microchannel flow boiling have observed explosive bubble growth, e.g. [6,29,39,40]. The large liquid superheat at the location of bubble nucleation is responsible for this explosive growth causing instabilities and flow reversal. Placing inlet restrictors and introducing nucleation cavities of radii satisfying nucleation criteria are some of the solutions offered to eliminate or mitigate this behavior.

2.3.3. Elongated bubble/slug flow

Following the explosive growth, the vapor surrounded by a thin liquid film on the wall occupies the entire channel as an elongated bubble. The upstream interface dissipates the available liquid superheat and is followed by a slug of liquid until the next nucleation incidence occurs. This is seen to be a prevalent flow pattern in microchannel. Steinke and Kandlikar [29] conducted experiments in parallel rectangular copper microchannels with a hydraulic diameter of 207 μm using water over heat and mass flux ranges of 5–930 kW/m^2 and 157–1782 kg/m^{2}s respectively. They found that explosive boiling with nucleation followed by slug formation was observed in the entire range. Under certain conditions, the flow was unstable with severe flow reversal was observed with a high-speed camera. The heat transfer coefficient was very high near the inlet section and it decreased along the length of the microchannel. Similar observations are made by a number of investigators including Yen et al. [41] for water at a mass flux of 295 kg/m^{2}s and for the lower range of heat fluxes of 1–13 kW/m^{2}s and Hetsroni et al. [39].

Harirchian and Garimella [38] observed that at higher heat fluxes, the elongated bubble region is shortened and the flow enters annular flow regime. There is a liquid film around the vapor core in the bubble, which occasionally dries out before the next slug arrives.

2.3.4. Annular flow

The elongated bubble continues to grow in length as liquid evaporates from the film on the channel walls and the upstream and downstream interfaces. Sometimes the downstream slug is consumed or breaks off forming the annular flow. The liquid film thickness and heat transfer in this mode continue to be a topic of current research.

2.4. Characteristics of elongated bubble/slug flow pattern

The behavior of the liquid–vapor interface of a nucleating bubble as it expands into an elongated bubble and transitions into annular flow is critical to understanding the flow boiling phenomenon in microchannels. In this regard, numerical simulation of the interface region provides useful information. Son et al. [42] and Mukherjee and Dhir [43] developed a numerical scheme to study the growth and heat transfer associated with the liquid–vapor interface of nucleating bubbles and their merger. Mukherjee and Kandlikar [44]

extended this model to study the effect of advancing and receding contact angles and showed that the transient conduction and local liquid circulation play an important role in the removal of heat and its dissipation through the phase change process at the interface.

Fig. 6 shows the results for bubble growth in water in a microchannel. The nucleating bubble grows rapidly within less than 0.3 ms to form an elongated bubble. The bulk liquid is in a superheated state and its energy is being released through rapid evaporation at the interface. The numerical results from ref. [44] are depicted in the same figure along with the photographic images obtained in ref. [45], showing good qualitative agreement between the two. Comparing the sequential frames shown in Fig. 6, it is seen that the receding interface on the right side moves faster in the flow direction and eventually leads to an elongated bubble shape. The receding interface leaves behind a thinning layer of liquid wedge on the wall. The liquid film is superheated from the transient conduction while it was part of the liquid slug. This superheat is dissipated through evaporation, while the remaining film interacts thermally with the wall and the vapor core. The growth and movement of a bubble taking the elongated shape and its rapid movement downstream (toward right) is depicted in Fig. 7 [44].

The interface on the left side of the bubble in Fig. 7 faces upstream liquid which is cooler, causing the evaporation rate to slow down. The interface may recede backward if the upstream compressibility (including parallel channel effects) permits this movement. The interface eventually begins to advance in the flow direction. For systems with low upstream compressibility, the vapor sometimes moves backward through the liquid core, while liquid film flow proceeds in the flow direction [29]. For smaller diameter microchannels and at higher heat fluxes with inlet stabilizers, this behavior is not seen. As the advancing interface passes over the channel wall, heat is transferred by transient conduction from the wall to the liquid, and the nucleation cavity once again produces a bubble, continuing the cycle. The liquid is trapped as a slug between the advancing interface of the previous elongated bubble and the receding interface of the new bubble as shown in Fig. 8. The length of the liquid slug depends on the flow velocity and the time interval between the two successive nucleation events. At higher heat fluxes, multiple bubbles are seen to form on the heater surface. These bubbles coalesce and form larger bubbles and eventually transform into slug and annular flow patterns [37,38]. For the case of annular flow pattern, presence of a thick film is not beneficial for heat transfer. In such cases, it would be desirable to have a slug flow pattern with rapid succession of liquid and elongated vapor bubbles.

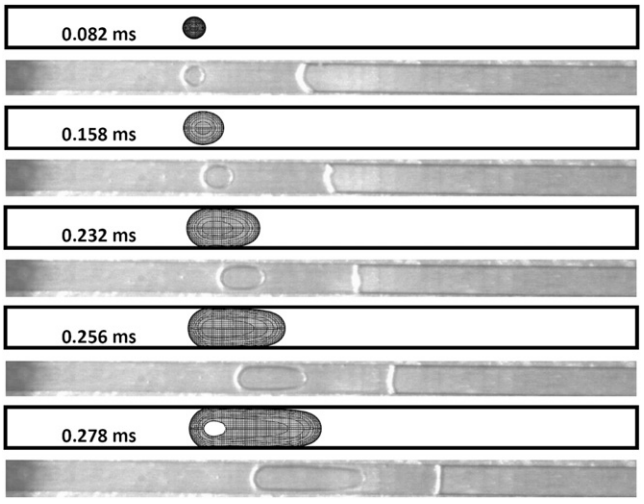

Fig. 6. Growth of a nucleating bubble into an elongated bubble during flow boiling of water inside a microchannel. Numerical simulation results, upper frames [44], and experimental visualization lower frames [45].

2.5. Stability and flow pattern consideration

The flow patterns and stability during flow boiling are the result of the forces acting on the evaporating interfaces in a microchannel. In this section, the forces discussed above are used to represent the stability and flow pattern transitions.

Unstable operation during flow boiling in microchannels is reported by a number of investigators [e.g. 4,6–9,22,29,37,39,40,45]. Before looking into stability criteria, it would be instructive to briefly review other microscale applications where scaling analysis provides useful transition criteria for processes involving liquid–vapor/gas interfaces. Two such applications that are discussed below are the formation of droplets or bubbles in microchannels and the transport of water through a fibrous gas diffusion layer matrix for fuel cell application.

The subject of droplet and bubble formation in microfluidic T-junctions has been extensively studied. Thorsen et al. [46] postulated that the droplet breakup is a result of the surface tension and shear forces acting on the droplet interface. However using a scaling analysis, Garstecki et al. [47] developed a model that showed that at low capillary numbers the droplet breakup is independent of the surface tension and viscosity of both the fluids. The only controlling parameters were identified as the channel geometry and the flow rates of the two streams. For a given total pressure drop of the gas flow, the flow rate is dependent on the length and the viscosity of the fluid, but the important parameter is the gas flow rate. Further confirmation of this hypothesis was obtained by Christopher et al. [48], who showed that the viscosity ratio did not play a role unless this ratio was close to 1. An excellent review on this topic is given by Christopher and Anna [49]. More recently, such a force balance and scaling analysis was used by Song et al. [50] for droplet splitting and liquid dispensing in electrowetting-on-dielectric microfluidic actuators.

Another application where scaling analysis is being actively pursued is the flow of water in the gas diffusion layer of a Proton Exchange Membrane fuel cell in the presence of a countercurrent flow of reactant gases. In porous medium applications, capillary number and viscosity ratio of the two fluids are used to generate a phase diagram that distinguishes between the capillary fingering, viscous fingering and stable displacement [51]. Recent efforts are under way to extend this diagram for the fibrous gas diffusion layer material. Additional effects due to varying surface energy (contact angle) within the matrix makes the task even more challenging, but the scaling parameters for porous medium seem to be applicable in fibrous applications as well [52].

In studying flow pattern transitions, Lee and Pan [53] conducted careful flow visualization experiments with water in 99.8 μm wide and 20.3 μm deep silicon microchannels over heat and mass flux ranges of 14.9–372 kW/m^2 and 417–625 kg/m^{2}s. Using frame rates up to 50,000 fps, they confirmed that bubbles nucleated over specific cavities and then rapidly grew into slugs. Bubbly flow was not observed under any operating conditions. The nucleation onset followed the established nucleation criterion of Hsu [54] and corresponded to the cavity diameters available on the heater surface.

Flow patterns have been a topic of great interest during flow boiling in microchannels. A recent study of channel dimensions and heat and mass fluxes on flow patterns and heat transfer is reported by Harirchian and Garimella [38]. They conducted experiments with FC-77 in 400 μm deep channels with widths varying from 100 μm to 5850 μm. They observed that the flow patterns and heat transfer trends were similar for channel wider than 400 μm, while a distinct change was noted for 100 μm wide microchannels. The bubble nucleation followed by bubbly flow was suppressed in these

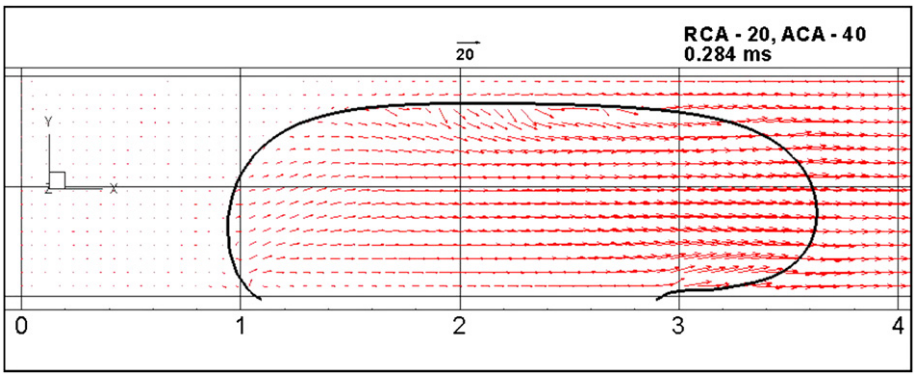

Fig. 7. Numerical simulation of bubble growth in a 200 μm square microchannel showing receding (right) and advancing (left) liquid–vapor interfaces [44].

microchannels and slug flow was noted to be the dominant flow pattern, followed by churn/annular flow. As the mass flux increased, the slug flow was more prevalent, while increasing heat flux resulted in churn/annular flow. All the data sets were obtained under stable operating conditions.

The stability of flow boiling has been a focus of a number of investigations. Incorporating pressure drop restrictors at the inlet to each channel and providing artificial nucleation cavities stabilized the boiling in microchannels [22,55]. Consolini and Thome [56] recently considered the convective heat transfer in the presence of flow instabilities. Wang et al. [57] found that the effects of inlet and outlet headers had a significant effect on the flow boiling stability. Cheng et al. [58] provide an excellent overview of the stability and flow patterns in small hydraulic diameter rectangular channels. Wang et al. [37] conducted experiments to identify the stable and unstable regions and proposed a map which shows that the flow is stable only in the region $q/G < 0.96$ kJ/kg. The region $q/G > 2.14$ kJ/kg was unstable with short-period oscillations and the intermediate region $0.96 < q/G < 0.2.14$ kJ/kg was unstable with long-period oscillations. These regions were associated with specific flow patterns.

As a bubble nucleates and occupies the entire channel, the stability of the flow depends on the balance of the inertia force of the liquid and the evaporation momentum force at the liquid–vapor interface between the expanding bubble and the upstream liquid. The ratio of these forces is given by the parameter K_1 introduced by Kandlikar [17].

$$K_1 = \frac{\text{Evap}\cdot\text{Mom Force}}{\text{Interia Force}} = \frac{\left(\frac{q}{Gh_{fg}}\right)^2\left(\frac{D}{\rho_V}\right)}{\left(\frac{G^2D}{\rho_L}\right)} = \left(\frac{q}{Gh_{fg}}\right)^2\left(\frac{\rho_L}{\rho_V}\right) \quad (16)$$

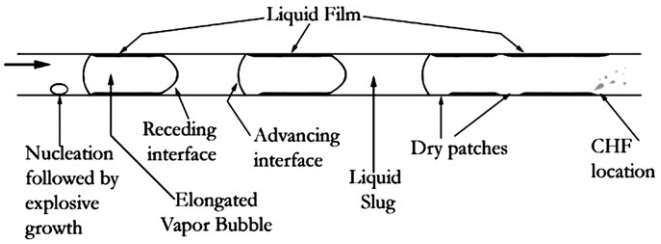

Fig. 8. Representation of different heat transfer mechanisms during elongated bubble/slug flow patterns showing similarities between nucleate pool boiling and flow boiling in microchannels.

Following the criteria proposed by Wang et al. [37], and introducing the properties of water at the mean test section pressure employed, which was quite close to 1 bar, the stability criteria and the associated flow patterns may be expressed as follows:

Stable boiling, steady bubbly/slug flow: $K_1 \leq 2.9 \times 10^{-4}$.

Unstable boiling with short-period oscillations, bubbly/annular alternating: $2.9 \times 10^{-4} < K_1 < 1.45 \times 10^{-3}$.

Unstable boiling with long-period oscillations, annular/mist alternating: $K_1 \geq 1.45 \times 10^{-3}$.

Wang et al. [57] also found that the type of inlet headers further modified the boundaries between the two regions. The results for transitions among flow patterns from Wang et al. [37] and Wang et al. [57] were both presented on a plot of q vs. G. When the recent data for FC-77 from Harirchian and Garimella [38] was plotted on this map, it resulted in extremely large deviations since the q/G values employed in FC-77 systems are significantly lower as compared to water. These maps are replotted using the evaporation momentum and inertia forces with the scaling parameter K_1 as the transition criterion. Fig. 9(a) and (b) show the data from Wang et al. [37] and Wang et al. [57] respectively. It is seen that the transition criteria are slightly different between the two header configurations. The data of Harirchian and Garimella [38] is plotted on this map in Fig. 9(c). It is seen that the entire data set is well represented on the map and the transition boundaries for the vertical inlet header configuration from Wang et al. [37] are able to accurately represent the flow pattern transitions using the parameter K_1.

The size and shape of the microchannel also influence the transition criteria shown in Fig. 9(c). Furthermore, different nucleation characteristics on the wall also play a significant role in flow pattern development. The flow pattern transition and stability map presented in Fig. 9(a)–(c) are expected to undergo changes to accommodate these factors as additional data become available.

3. Mechanistic description of flow boiling

3.1. Heat transfer to the liquid slug trapped between two elongated bubbles

Heat transfer to the liquid slug trapped between two elongated bubbles, as seen in Fig. 8, was simulated experimentally and numerically by a steady meniscus formed on a moving heated surface [59,60]. Liquid is supplied at a nozzle outlet kept at a close distance from the heated surface. Fig. 10 shows a photograph of the meniscus formed between a nozzle and a heated, rotating copper surface [59]. The liquid circulation and temperature contours

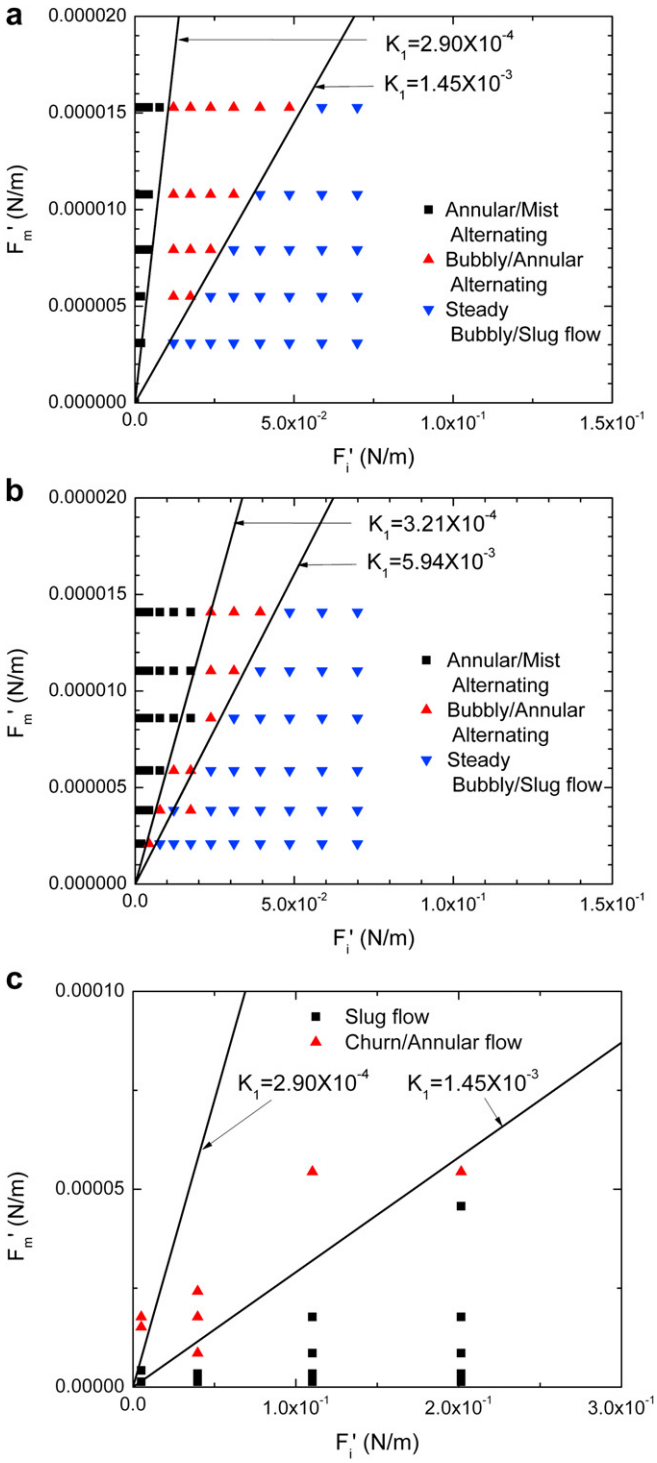

Fig. 9. Flow pattern transition and stability map using evaporation momentum and inertia forces and Wang et al. [37] criteria; (a) water data of Wang et al. [37] with vertical (normal) headers, $D_h = 186$ μm, (b) water data of Wang et al. [57] with vertical (normal) headers, $D_h = 186$ μm, (c) FC-77 data of Harirchian and Garimella [38], $D_h = 100$ μm.

within a moving meniscus were also numerically obtained and are shown in Fig. 11.

The liquid front at the advancing interface covers the heater surface and the resulting transient heat transfer is very high at the leading edge and slowly decreases toward the receding edge. This is confirmed by the steep temperature gradient near the wall at the left interface. On the right side, the meniscus is receding and the

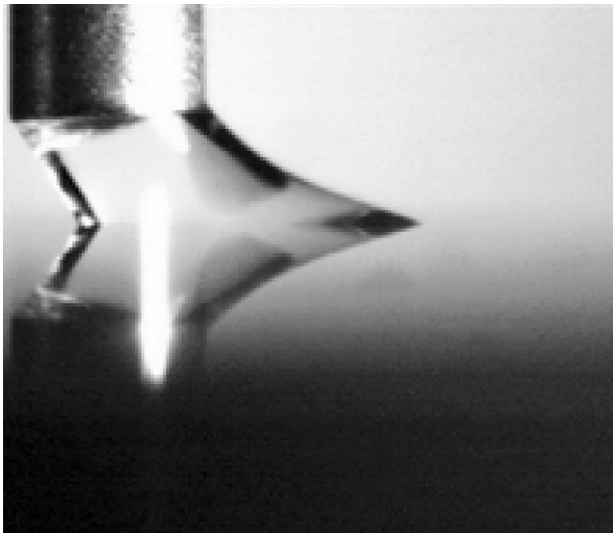

Fig. 10. Photograph of an evaporating water meniscus on a polished rotating copper heater showing the advancing (left) and receding (right) interfaces [59].

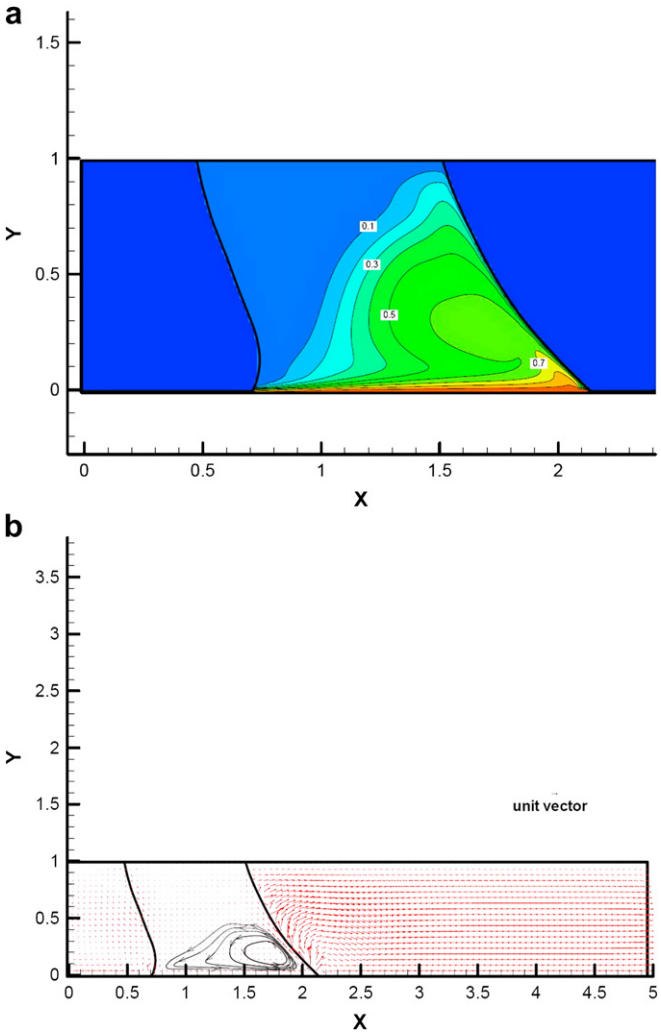

Fig. 11. Liquid temperature profile (a) and velocity vectors (b) inside a meniscus (moving from right to left at a velocity of 0.1 m/s) over a heated surface. Contact angles advancing, left interface, $\theta_A = 61°$, receding, right interface, $\theta_R = 48°$ [60].

heated liquid from the boundary layer formed over the heater circulates behind the liquid–vapor interface and results in significant evaporation. Thus transient conduction followed by release of energy through evaporation at the interface is identified as the heat transfer mechanism in this configuration.

Comparing the moving menisci with the slug flow, it is seen that the two mechanisms are similar. Fig. 8 shows the liquid slug trapped between the two successive elongated bubbles in a microchannel. This description resembles with the three-zone model originally proposed by Jacobi and Thome [18]. However, the heat transfer in each region is considered here by comparing its relative counterpart in pool boiling. At the advancing interface in the slug, liquid comes in contact with the wall, which may be partially dry or may be covered with a thin liquid film. The liquid behind the interface begins to be heated due to transient conduction, and sweeps over the receding interface resulting in significant evaporation, similar to the receding meniscus on a heated surface shown in Fig. 10. In case of complete dryout of the film, there may be an additional component due to enhanced heat transfer at the triple line, but this contribution is expected to be quite small.

4. Comparison between pool boiling and microchannel flow boiling mechanisms

Significant advances have been made in recent years in our understanding of pool boiling heat transfer. Demiray and Kim [61] and Myers et al. [62] conducted extensive microscale experiments with dielectric fluids using an array of microheaters with 100 μm resolution and studied the transient heat transfer process on the heater surface during the bubble ebullition cycle. The individual heaters were controlled to provide a desired constant heat flux or constant temperature boundary condition. These studies provide highly time- and space-resolved descriptions of the heat transfer process.

Based on their experimental observations, Demiray and Kim [61] and Myers et al. [62] determined the contributions from different mechanisms during pool boiling. As the nucleating bubble grows, heat is transferred by evaporation from the microlayer. Its contribution reduces significantly as the microlayer evaporates completely, leaving dry patches at some locations resulting in a very low heat transfer over the patches. As the bubble begins to depart, the liquid interface then advances and covers the surface. This results in a significantly higher heat transfer rate due to transient heat conduction to the liquid. In case where the liquid film is still present, the advancing liquid replenishes the film with cooler liquid and is able to provide a higher heat transfer due to transient conduction mode. As the bubble departs, the liquid covers the entire heating surface and is heated further from transient conduction forming a superheated liquid layer over the heater surface. The cycle begins again with the nucleation of the next bubble. The superheated liquid layer releases its energy by evaporation at the receding liquid–vapor interface during the growth period of the following bubble. The dominant mode of heat transfer was found to be transient conduction. The microlayer evaporation contribution was found to be quite small, around 20–25 percent, confirming the numerical results of Son et al. [42].

Fig. 12(a) and (b) from Myers et al. [62] are redrawn from the original data to show the contributions from different mechanisms. The transient conduction raises the liquid superheat, which is released at the evaporating interface through microconvection. Thus these two mechanisms of transient conduction and microconvection are coupled and hence are combined. It is seen from Fig. 12(a) that the microlayer evaporation begins following the bubble nucleation and ends with the appearance of dry spots. The energy transferred by microlayer evaporation is depicted in

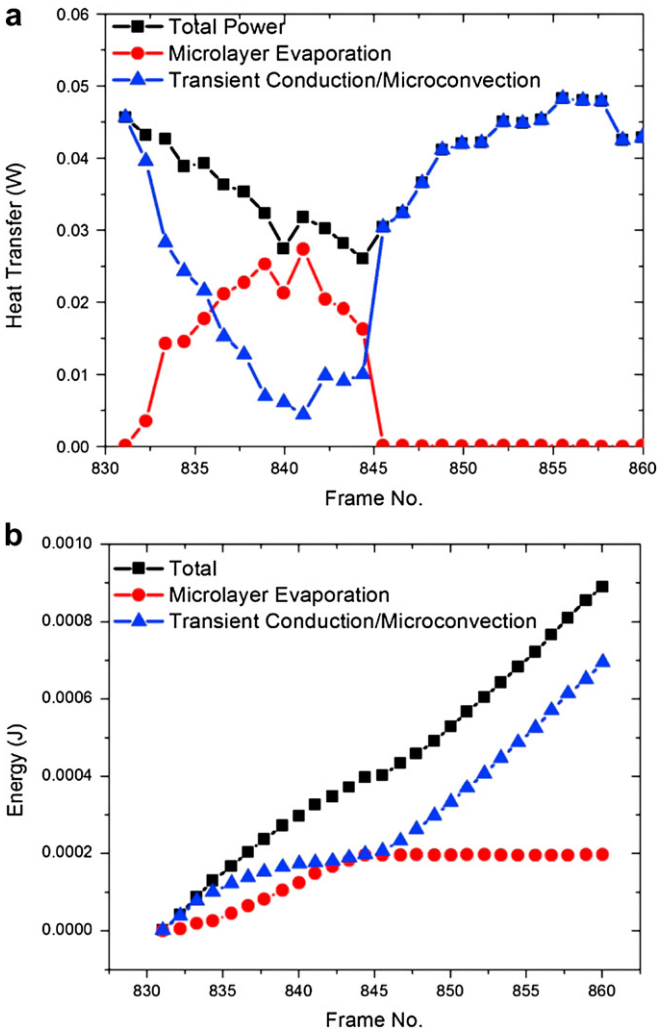

Fig. 12. Contributions to (a) local heat transfer rate and (b) total energy transferred from the different mechanisms during nucleate pool boiling under a single bubble, redrawn from Myers et al. [62].

Fig. 12(b) and is seen to be 22 percent of the total energy transfer. This value is in agreement with the numerical results of Son et al. [42], who estimated the microlayer contribution to be around 20 percent. Transient conduction occurs in both cases when the liquid film has been completely dried out, as well as when there is a film left behind. The advancing liquid brings cooler liquid to the heater surface in both cases.

Recent publications by Moghaddam and Kiger [63,64] on visualization and simultaneous local heat transfer measurements under a nucleating bubble through its entire cycle provide additional useful information. The microlayer contribution was divided between the conduction from the heater and evaporation from the initial superheat of the liquid film. It was shown that the initial superheat was also an important contributor to the heat transfer. The overall contribution from the microlayer evaporation was in agreement with earlier results and was also found to be around 20 percent of the total heat transfer.

Another aspect that was highlighted by Moghaddam and Kiger [63,64] was that the microconvection played a greater role at higher liquid wall temperatures. An increase in waiting time resulted in an explosive bubble growth and an increased contribution from the transient conduction mode. The transient conduction was modeled somewhat differently, allowing for a gradual rewetting front as the

bubble interface recedes prior to departure. This is different from the transient conduction model of Mikic and Rohsenow [65] in which the bulk liquid replaced the entire active area equivalent to two times the departure bubble diameter. The findings by Moghaddam and Kiger indicate that the area for transient conduction is restricted to about half the departure bubble diameter.

When comparing the nucleate pool boiling with flow boiling following nucleation of a bubble, significant similarities are noted. In both systems, a nucleating vapor bubble grows from the evaporation at the bulk liquid–vapor interface, which provides a relaxation mechanism for liquid superheat in the surrounding liquid. Evaporation from the interface leads to an elongated bubble in microchannel flow boiling, and the heater surface surrounding the vapor is covered with a microlayer, similar to the microlayer under a bubble in pool boiling. The receding and advancing menisci at the front and back of the elongated bubble are similar to the interfaces during growth and departure phases of a nucleating bubble in pool boiling respectively. The transient conduction mechanism during pool boiling during the departure mode is replaced by the transient heat conduction to the slug trapped between the two elongated menisci. Note that the heat transfer in the liquid slug is quite complex due to transient conduction at the wall; microconvection induces circulation within the slug and evaporation at the receding interface upstream. Because of these microconvection and evaporation features, heat transfer in the liquid slugs is quite different from the conventional entry-region problem. Furthermore, the liquid slug is continuously accelerating due to evaporation in the elongated bubble following behind it upstream. The liquid mass in the slug is also constantly being depleted due to evaporation at the interfaces, mainly the receding interface, and liquid supply for the formation of the liquid film.

Another observation can be made regarding the contribution from the microconvection mechanism. It provides a pathway for heat to be transported from the superheated liquid layer experiencing transient conduction to the liquid–vapor interface of the receding interface. This also helps to increase the heat transfer rate by reducing the temperature of the liquid behind the advancing interface experiencing transient conduction.

4.1. Microlayer characteristics

The microlayer formed in pool boiling has been studied extensively. One of the early works by Koffman and Plesset [66] indicates that the thickness is on the order of 1–5 μm under a nucleating bubble. Due to evaporation, it assumes a wedge shape under a bubble, and often forms a dry spot in the center at high heat fluxes as the microlayer is depleted. Moriyama and Inoue [67] reported a measured microlayer thickness of 5 μm in a narrow gap of 0.4 mm with R-134a. Their thickness predictive model was used by Revellin et al. [68].

Recent work by Zhang et al. [69] provides useful information on liquid film thickness measurement using laser extinction method in a microgap as a function of interface velocity. An interesting observation made from these experiments was that the film thickness increased with the velocity of the interface. For the interface velocities of 3–5 m/s, the thickness was around 10 μm for water and 20 μm for ethanol and toluene.

The film thickness in flow boiling in microchannels is expected to be higher during explosive boiling due to higher interface velocities. The contribution from the microlayer evaporation will therefore be smaller as compared to the pool boiling, where it contributes approximately 20 percent to the total heat transferred. The dryout of the microlayer has also been observed under the elongated bubble in flow boiling by many investigators, including recently by Wang et al. [57] for water in 186 μm hydraulic diameter parallel channels. These features are identified as some of the limiting characteristics of flow boiling in microchannels. A more comprehensive comparison between pool boiling and microchannel flow boiling is presented in [70].

4.2. Contribution from convective boiling mechanism during microchannel flow boiling

Many researchers have discounted the convective contribution by observing that the heat transfer coefficient during flow boiling in microchannels is independent of the mass flux. This reasoning assumes that the convective heat transfer increases with mass flow rate, which is true in the case of turbulent flow. But in the case of laminar flow, as is the case in microchannels over most of the operating conditions tested, the heat transfer coefficient is independent of the flow rate. (Although some effect may be present due to developing flow and two-phase mixing). Furthermore, the variation of heat transfer coefficient with quality depends on the boiling number as well as density ratio, providing increasing, flat, or decreasing trends at low qualities [71].

It is therefore reasonable to use a flow boiling correlation that includes the convective contribution, and recognizes the increased nucleate boiling contribution. The correlation by Kandlikar and Balasubramanian [72] accounts for the increased contribution from the nucleate boiling mechanism, and the reduced dependence on the mass flux in the transition region, and a constant heat transfer coefficient in the laminar region as identified by the respective Reynolds number ranges. Fig. 13 shows a comparison of the flow boiling data for R141b in 60 μm × 200 μm silicon microchannels with the correlation as reported by Dong et al. [73]. Yen et al. [41] also reported good agreement of their R123 flow boiling data in 190 μm diameter microtubes with the nucleate boiling component of the original Kandlikar [74] correlation. Further improvements in the correlation will be needed to better incorporate the turbulence transition due to the two-phase flow effects and to derive the appropriate values of the fluid-surface parameter F_{FI} for new fluids tested in microchannels as these values are not reported in the correlation. Also, the correlation by Kandlikar and Balasubramanian [72] was developed as an extension of an earlier correlation [74]. It incorporates the boiling number and density ratio, but not explicitly as the group K_1. It may be beneficial to consider the new property group K_1 in developing future correlations.

Another aspect of interest is the trend of h vs. x. This topic has been discussed extensively in literature. A flow boiling map was presented by Kandlikar [71] to address this issue. This trend is the result of the

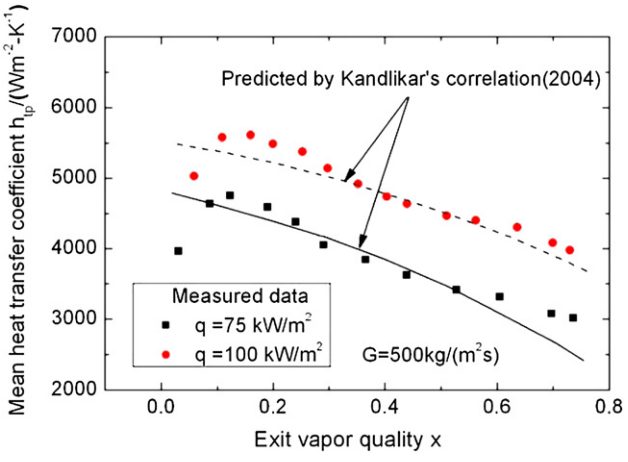

Fig. 13. Comparison of the flow boiling data for R141b in 60 μm × 200 μm silicon microchannels with the correlation by Kandlikar and Balasubramanian [72].

combination of the nucleate boiling component, which decreases with x, and the convective contribution, which increases with x. This increase depends on the density ratio – a larger value will provide a greater increase due to a higher flow velocity upon evaporation. The net result then depends on the relative contribution from these two components. As stated earlier, the increase in velocity in laminar flow encountered in microchannels may not yield a higher heat transfer coefficient with an increase in flow velocity. As a result, the trend of h vs. x in microchannels would tend to be flatter or decreasing as compared to the minichannels or macrochannels.

5. Recommendations for future research

- The elongated bubble flow pattern is seen to be a limiting factor in the heat transfer during flow boiling in microchannels. It is recommended that this flow pattern be avoided or delayed by nucleating bubbles in the flow while the bulk flow is still subcooled. This can be accomplished by providing nucleation sites in the hotter regions of a rectangular microchannel, such as corners. A schematic showing the flow pattern changes with nucleation under subcooled conditions is depicted in Fig. 14.
- Microbubble Emission Boiling (MEB), described by Hirono et al. [75] provides high heat transfer coefficients at higher heat fluxes in the transient boiling region. It is attractive in microchannel flow boiling in the regions where local dryout regions occur. Preliminary work in this field seems promising [76] and is recommended for further exploration.
- The next recommendation deals with the dryout region. It is recommended that the dryout be delayed by providing hydrophilic walls that draw liquid away from the corner regions of a microchannel as shown in Fig. 15. Recent studies conducted on the surface energy effects on pool boiling, e.g. Phan et al. [77] may be extended to microchannel flow boiling systems. Another investigation by Khanikar et al. [78] employing carbon nanotubes coating on the 10-mm wide and 371 μm high minichannel heated wall showed an increase in pressure drop and an increase in instability. A systematic study with microchannels equipped with flow stabilization features, such as restrictors and specific nucleation sites, and nanostructures is recommended.
- It is recommended that the local temperature under an elongated bubble and liquid slug be measured using the advanced microfabrication technology that has been employed in pool boiling by pioneering work by researchers such as [61,62], or more recently by [63,64]. The application of liquid crystal thermography [79] and infrared visualization [80,81] of the substrate to obtain local temperature data with simultaneous flow visualization in microchannels are promising new techniques which could be implemented to reveal the interrelationships between the two-phase flow dynamics and local heat transfer. Such information would be immensely useful in identifying new directions for enhancing heat transfer.

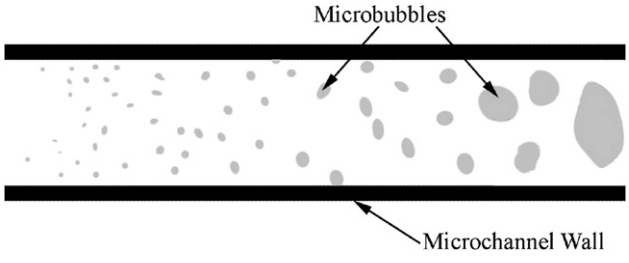

Fig. 14. Microbubbles nucleating in subcooled liquid and forming bubbly flow in a microchannel.

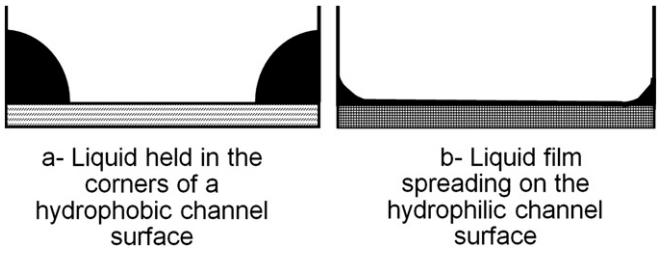

Fig. 15. Spreading of liquid film to delay localized dryout by spreading liquid held in the corners as film on the channel walls.

6. Conclusions

Recent developments in single-phase flow in enhanced microchannels have provided significantly higher performance with high heat flux dissipation and high heat transfer coefficients. In order to improve the performance of flow boiling systems with microchannels to match and exceed this level, a fundamental understanding of the underlying transport processes is needed. A scaling analysis of the forces indicates that surface tension and evaporation momentum forces play a dominant role at microscale. Application of the scaling analysis to identify flow region transitions provided encouraging results. Elongated bubble/slug flow pattern is seen to be dominant in microchannels. Heat transfer under this flow pattern is seen to be similar to that around a nucleating bubble in pool boiling. The receding and advancing fronts of the elongated bubble are similar to the respective interfaces of a nucleating bubble during growth and departure phases. Transient conduction/microconvection is identified as the major heat transfer mechanism associated with the elongated bubble/slug flow pattern. Since the liquid flow is laminar in microchannels under the operating conditions of engineering interest, the mass flux independence seen in the flow boiling data may not necessarily indicate the absence of convective boiling component. Further research on identifying the effects of turbulence transition in two-phase flow is suggested. Future research is recommended on (i) altering nucleation patterns through strategic placement of nucleation sites, (ii) application of microbubble emission boiling (MEB) in highly subcooled flow, (iii) providing nanosurface coatings to enhance nucleation characteristics and reduce dryout, and (iii) use of liquid crystal and high speed infrared thermography to reveal local temperature fluctuations in conjunction of high speed flow visualization for developing heat transfer enhancing strategies.

Acknowledgement

The work was performed in the Thermal Analysis, Microfluidics and Fuel Cell Laboratory in the Mechanical Engineering Department at Rochester Institute of Technology.

References

[1] E.G. Colgan, B. Furman, M. Gaynes, W. Graham, N. LaBianca, J.H. Magerlein, R.J. Polastre, M.B. Rothwell, R.J. Bezama, R. Choudhary, K. Marston, H. Toy, J. Wakil, J. Zitz, R. Schmidt, A practical implementation of silicon microchannel coolers for high power chips. IEEE Transactions on Components and Packaging Technologies 30 (2007) 218–225.
[2] M.E. Steinke, S.G. Kandlikar, Single-phase liquid heat transfer in plain and enhanced microchannels, Proceedings of the ASME 4th International Conference on Nanochannels, Microchannels and Minichannels, ICNMM2006, 2006, pp. 943–951.
[3] C.B. Sobhan, S.V. Garimella, A comparative analysis of studies on heat transfer and fluid flow in microchannels. Microscale Thermophysical Engineering 5 (2001) 293–311.
[4] S.G. Kandlikar, Fundamental issues related to flow boiling in minichannels and microchannels. Experimental Thermal and Fluid Science 26 (2002) 389–407.

[5] S.G. Kandlikar, Two-phase flow patterns, pressure drop and heat transfer during boiling in minichannel and microchannel flow passages of compact evaporators. Heat Transfer Engineering 23 (2002) 5–23.
[6] A. Serizawa, Z. Feng, Z. Kawara, Two-phase flow in microchannels. Experimental Thermal and Fluid Science 26 (2002) 703–714.
[7] A.E. Bergles, J.H. Lienhard, G.E. Kendall, P. Griffith, Boiling and evaporation in small diameter channels. Heat Transfer Engineering 24 (2003) 18–40.
[8] S.V. Garimella, C.B. Sobhan, Transport in microchannels—a critical review. Annual Reviews in Heat Transfer 13 (2003) 1–50.
[9] J.R. Thome, Boiling in microchannels. International Journal of Heat and Fluid Flow 255 (2004) 128–139.
[10] B. Agostini, M. Fabbri, J.E. Park, L. Wojtan, J.R. Thome, B. Michel, State of the art of high heat flux cooling technologies. Heat Transfer Engineering 28 (2007) 258–281.
[11] S.S. Bertsch, E.A. Groll, S.V. Garimella, Review and comparative analysis of studies on saturated flow boiling in small channels. Nanoscale and Microscale Thermophysical Engineering 12 (2008) 187–227.
[12] W. Nakayama, T. Daikoku, H. Kuwahara, T. Nakajima, Dynamic model of enhanced boiling heat transfer on porous surfaces. Journal of Heat Transfer 102 (1980) 445–449.
[13] H. Pantisidis, R.D. Gresham, J.W. Westwater, Boiling of liquids in a compact plate-fin heat exchanger. International Journal of Heat and Mass Transfer 18 (1975) 37–42.
[14] J.C. Khanpara, A.E. Bergles, M.B. Pate, Augmentation of R-l 13 in-tube evaporation with micro-fin tubes. ASHRAE Transactions 92 (Pt. 2) (1986) 506–524.
[15] Y.P. Peles, S. Haber, A steady, one dimensional model for boiling two-phase flow in triangular microchannel. International Journal of Multiphase Flow 26 (2000) 1095–1115.
[16] U. Imke, Porous media simplified simulation of single- and two-phase flow heat transfer in micro-channel heat exchangers. Chemical Engineering Journal 101 (2004) 295–302.
[17] S.G. Kandlikar, Heat transfer mechanisms during flow boiling in microchannels. Journal of Heat Transfer 126 (2004) 8–16.
[18] J.R. Thome, V. Dupont, A.M. Jacobi, Heat transfer model for evaporation in microchannels, part I: presentation of the model. International Journal of Heat and Mass Transfer 47 (2004) 3375–3385.
[19] J.R. Thome, V. Dupont, A.M. Jacobi, Heat transfer model for evaporation in microchannels, part II: comparison with the database. International Journal of Heat and Mass Transfer 47 (2004) 3387–3401.
[20] J. Xu, Y. Gan, D. Zhang, X. Li, Microscale boiling heat transfer in a micro-timescale at high heat fluxes. Journal of Micromechanics and Microengineering 15 (2005) 362–376.
[21] L. Zhang, E.N. Wang, K.E. Goodson, T.W. Kenny, Phase change phenomena in silicon microchannels. International Journal of Heat and Mass Transfer 48 (2005) 1572–1582.
[22] S.G. Kandlikar, Nucleation characteristics and stability considerations during flow boiling in microchannels. Experimental Thermal and Fluid Science 30 (2006) 441–447.
[23] G. Ribatski, L. Wojtan, J.R. Thome, An analysis of experimental data and prediction methods for two-phase frictional pressure drop and flow boiling heat transfer in micro-scale channels. Experimental Thermal and Fluid Science 31 (2006) 1–19.
[24] Y. Gan, J. Xu, S. Wang, Are the available boiling heat transfer coefficients suitable for silicon microchannel heat sinks? Microfluidics Nanofluidics 4 (2008) 575–587.
[25] A. Ullmann, N. Brauner, The prediction of flow pattern maps in minichannels. Multiphase Science and Technology 19 (2007) 49–73.
[26] P.A. Kew, K. Cornwell, Correlations for the prediction of boiling heat transfer in small-diameter channels. Applied Thermal Engineering 17 (1997) 705–715.
[27] S.G. Kandlikar, W.J. Grande, Evolution of microchannel flow passages – thermohydraulic performance and fabrication technology. Heat Transfer Engineering 24 (2003) 3–17.
[28] S.G. Kandlikar, A theoretical model to predict pool boiling CHF incorporating effects of contact angle and orientation. Journal of Heat Transfer 123 (2001) 1071–1079.
[29] M.E. Steinke, S.G. Kandlikar, An experimental investigation of flow boiling characteristics of water in parallel microchannels. Journal of Heat Transfer 126 (2004) 518–526.
[30] A. Kosar, Y. Peles, A.E. Bergles, G.S. Cole, Experimental investigation of critical heat flux in microchannels for flow-field Probes, ICNMM09–82214, 10pp, ASME Seventh International Conference on Nanochannels, Microchannels and Minichannels, June 22–24, Pohang, Korea, 2009.
[31] M. Tange, M. Watanabe, S. Takagi, F. Tekemura, M. Shoji, Microbubble emission boiling in a rectangular channel Flow, ASME ICMM 2005, 3rd International Conference on Microchannels, and Minichannels, Toronto, 2005, pp. 139–143.
[32] C. Li, Z. Wang, P.I. Wang, Y. Peles, N. Koratkar, G.P. Peterson, Nanostructured copper interfaces for enhanced boiling. SMALL 4 (No. 8) (2008) 1084–1088.
[33] T.S. Zhao, Q.C. Bi, Co-current air-water two-phase flow patterns in triangular microchannels. International Journal of Multiphase Flow 27 (2001) 765–782.
[34] E. Sobierska, R. Kulenovic, R. Mertz, Heat transfer mechanism and flow pattern during flow boiling of water in a vertical narrow channel – experimental results. International Journal of Thermal Sciences 46 (2007) 1172–1181.
[35] R. Revellin, V. Dupont, T. Ursenbacher, J.R. Thome, I. Zun, Characterization of diabatic two-phase flows in microchannels: flow parameter results for R-134a in a 0.5 mm channel. International Journal of Multiphase Flow 32 (2006) 755–774.
[36] A. Kawahara, P.M.-Y. Chung, M. Kawaji, Investigation of two-phase flow pattern, void fraction, and pressure drop in a microchannel. International Journal of Multiphase Flow 28 (2002) 1141–1435.
[37] G.D. Wang, P. Cheng, H.Y. Wu, Unstable and stable flow boiling in parallel microchannels and in a single microchannel. International Journal of Heat and Mass Transfer 50 (2007) 4297–4310.
[38] T. Harirchian, S.V. Garimella, Effects of channel dimension, heat flux, and mass flux on flow boiling regimes in microchannels. International Journal of Multiphase Flow 35 (2009) 349–362.
[39] G. Hetsroni, A. Mosyak, E. Pogrebnyak, Z. Segal, Explosive boiling in parallel microchannels. International Journal of Multiphase Flow 31 (2005) 371–392.
[40] C.-J. Kuo, Y. Peles, Flow boiling instabilities in microchannels and means for mitigation by reentrant cavities. Journal of Heat Transfer 130 (Article No. 072402) (2008) 10.
[41] T.-H. Yen, N. Kasagi, Y. Suzuki, Forced convective boiling heat transfer in microtubes at low mass and heat fluxes. International Journal of Multiphase Flow 29 (2003) 1771–1792.
[42] G. Son, V.K. Dhir, N. Ramanujapu, Dynamics and heat transfer associated with a single bubble during nucleate boiling on a horizontal surface. Journal of Heat Transfer 121 (1999) 623–629.
[43] A. Mukherjee, V.K. Dhir, Study of lateral merger of vapor during nucleate pool boiling. Journal of Heat Transfer 126 (2004) 1023–1039.
[44] A. Mukherjee, S.G. Kandlikar, Numerical simulation of growth of a vapor bubble during flow boiling of water in a microchannel. Microfluidics and Nanofluidics 1 (2005) 137–145.
[45] P. Balasubramanian, S.G. Kandlikar, Experimental study of flow patterns, pressure drop, and flow instabilities in parallel rectangular minichannels. Heat Transfer Engineering 26 (2005) 20–27.
[46] T. Thorsen, R.W. Roberts, F.H. Arnold, S.R. Quake, Dynamic pattern formation in a vesicle-generating microfluidic device. Physical Review Letters 86 (2001) 4163–4166.
[47] P. Garstecki, M.J. Fuerstman, H.A. Stone, G.M. Whitesides, Formation of droplets and bubbles in a microfluidic T-junction—scaling and mechanism of break-up. Lab on a Chip 6 (2006) 437–446.
[48] G.F. Christopher, N.N. Noharuddin, J.A. Taylor, S.L. Anna, Experimental observations of the squeezing-to-dripping transition in T-shaped microfluidic junctions. Physical Review E 78 (2008) 036317(12).
[49] G.F. Christopher, S.L. Anna, Microfluidic methods for generating continuous droplet streams. Journal of Physics D: Applied Physics 40 (2007) R319–R336.
[50] J.H. Song, R. Evans, Y.-Y. Lin, B.-N. Hsu, R.B. Fair, A scaling model for electrowetting-on-dielectric microfluidic actuators. Microfluidics and Nanofluidics 7 (2009) 75–89.
[51] R. Lenormand, E. Touboul, C. Zarcone, Numerical models and experiments on immiscible displacements in porous media. Journal of Fluid Mechanics 189 (1988) 165–187.
[52] E.F. Medici, J.S. Allen, Existence of the phase drainage diagram in proton exchange membrane fuel cell fibrous diffusion media. Journal of Power Sources 191 (2009) 417–427.
[53] P.C. Lee, C. Pan, On the eruptive boiling in silicon-based microchannels. International Journal of Heat and Mass Transfer 51 (2008) 4841–4849.
[54] Y.Y. Hsu, On the size range of active nucleation cavities on a heating surface. ASME Journal of Heat Transfer 84 (1962) 207–216.
[55] S.G. Kandlikar, W.K. Kuan, D.A. Willistein, J. Borrelli, Stabilization of flow boiling in microchannels using pressure drop elements and fabricated nucleation sites. Journal of Heat Transfer 128 (2006) 389–396.
[56] L. Consolini, J.R. Thome, Micro-channel convective boiling heat transfer with flow instabilities, ECI International Conference on Boiling Heat Transfer, Florianopolis, Brazil, 3–7 May, Paper MC1, 2009.
[57] W. Wang, P. Cheng, A.E. Bergles, Effect of inlet/outlet configurations on flow boiling instability in parallel microchannels. International Journal of Heat and Mass Transfer 51 (2008) 2267–2281.
[58] P. Cheng, G. Wang, X. Quan, Recent work on boiling and condensation. Journal of Heat Transfer 131 (043211) (2009) 15.
[59] S.G. Kandlikar, W.K. Kuan, A. Mukherjee, Experimental study of heat transfer in an evaporating meniscus on a moving heated surface. Journal of Heat Transfer 127 (2005) 244–252.
[60] A. Mukherjee, S.G. Kandlikar, Numerical study of an evaporating meniscus on a moving heated surface. Journal of Heat Transfer 128 (2006) 1285–1292.
[61] F. Demiray, J. Kim, Microscale heat transfer measurements during pool boiling of FC-72: effect of subcooling. International Journal of Heat and Mass Transfer 47 (2004) 3257–3268.
[62] J.G. Myers, V.K. Yerramilli, S.W. Hussey, G.F. Yee, J. Kim, Time and space resolved wall temperature and heat flux measurements during nucleate boiling with constant heat flux boundary conditions. International Journal of Heat and Mass Transfer 48 (2005) 2429–2442.
[63] S. Moghaddam, K. Kiger, Physical mechanisms of heat transfer during single bubble nucleate boiling of FC-72 under saturation conditions–I. Experimental investigation. International Journal of Heat and Mass Transfer 52 (2009) 1284–1294.
[64] S. Moghaddam, K. Kiger, Physical mechanisms of heat transfer during single bubble nucleate boiling of FC-72 under saturation conditions–II: theoretical analysis. International Journal of Heat and Mass Transfer 52 (2009) 1284–1294.
[65] B.B. Mikic, W.M. Rohsenow, A new correlation of pool boiling data including the effect of heating surface characteristics. Journal of Heat Transfer 91 (1969) 245–250.
[66] L.D. Koffman, M.S. Plesset, Experimental observations of the microlayer in vapor bubble growth on a heated solid. Journal of Heat Transfer 105 (1983) 625–632.

[67] K. Moriyama, A. Inoue, Thickness of the liquid film formed by a growing bubble in a narrow gap between two horizontal plates. Journal of Heat Transfer 118 (1996) 132–139.
[68] R. Revellin, B. Agostini, T. Ursenbacher, J.R. Thome, Experimental investigation of velocity and length of elongated bubbles for flow of R-134a in a 0.5 mm microchannel. Experimental Thermal and Fluid Science 32 (2008) 870–881.
[69] Y. Zhang, Y. Utaka, Kashiwabara, T. Kamiaka, Characteristics of microlayer thickness formed during boiling in microgaps, ICNMM09–82244, 6pp, ASME Seventh International Conference on Nanochannels, Microchannels and Minichannels, June 22–24, Pohang, Korea, 2009.
[70] S.G. Kandlikar, Similarities and difference between pool boiling and flow boiling heat transfer in microchannels. Heat Transfer Engineering 31 (3) (2010) 159–167.
[71] S.G. Kandlikar, Development of a flow boiling map for subcooled and saturated flow boiling of different fluids inside circular tubes. Journal of Heat Transfer 113 (1) (1991) 190–200.
[72] S.G. Kandlikar, P. Balasubramanian, An extension of the flow boiling correlation to transition, laminar and deep laminar flows in minichannels and microchannels. Heat Transfer Engineering 25 (2004) 86–93.
[73] T. Dong, Z. Yang, Q. Bi, Y. Zhang, Freon R141b flow boiling in silicon microchannel heat sinks: experimental investigation. Heat and Mass Transfer 44 (2008) 315–324.
[74] S.G. Kandlikar, A general correlation for two-phase flow boiling heat transfer inside horizontal and vertical tubes. Journal of Heat Transfer 112 (1990) 219–228.
[75] Y. Hirono, R. Shimada, S. Kumagai, T. Takeyama, Microbubbles emission boiling on a horizontal upward-facing rectangular surface in subcooled flow. JSME International Journal 30 (1987) 1282–1287.
[76] G. Wang, P. Cheng, Subccoled flow boiling and microbubble emission boiling phenomena in a partially heated microchannel. International Journal of Heat and Mass Transfer 52 (2009) 79–91.
[77] H.T. Phan, N. Caney, P. Marty, S. Colasson, J. Gavillet, A. Marechal, Influence of surface wettability on pool boiling heat transfer, ICNMM09–82030, 7pp, ASME Seventh International Conference on Nanochannels, Microchannels and Minichannels, June 22–24, Pohang, Korea, 2009.
[78] V. Khanikar, I. Mudawar, T. Fisher, Effects of carbon nanotube coating on flow boiling in a micro-channel. International Journal of Heat and Mass Transfer 52 (2009) 3805–3817.
[79] P. Stephan, T. Fuchs, Local heat flow and temperature fluctuations in wall and fluid in nucleate boiling systems. Heat and Mass Transfer 45 (2009) 919–928.
[80] J. Barber, K. Sefiane, D. Brutin, L. Tadrist, Hydrodynamics and heat transfer during flow boiling instabilities in a single microchannel. Applied Thermal Engineering 29 (2009) 1299–1308.
[81] P. Stephan, T. Fuchs, E. Wagner, N. Schweizer, Transient local heat Fluxes during the entire vapor bubble lifetime, Keynote Paper Presented at 7th ECI International Conference on Boiling Heat Transfer, Florianopolis-SC, Brazil, May 3–7, 2009.